Porphyrin−Dendrimer Assemblies Studied by Electronic Absorption Spectra and Time-Resolved Fluorescence

Pedro M. R. Paulo,[†] Roel Gronheid,[‡] Frans C. De Schryver,[‡] and Sílvia M. B. Costa*,[†]

Centro de Química Estrutural, Complexo 1, Instituto Superior Técnico, Av. Rovisco Pais, 1049-001 Lisboa, Portugal, and Department of Chemistry, Katholieke Universiteit Leuven, Celestijnenlaan 200 F, 3001 Heverlee, Belgium

Received June 20, 2003; Revised Manuscript Received September 2, 2003

ABSTRACT: Anionic *meso*-tetrakis(4-sulfonatophenyl)porphine (TSPP) interacts with poly(amido) amine (PAMAM) dendrimers of generations 2.0 and 4.0 in aqueous solution to form several dendrimer-associated species, which depend on the relative concentrations of dendrimer to porphyrin (D/P ≡ [PAMAM]/[TSPP]). At D/P ratios above the isoelectric point of the charge balance between the dendrimer and porphyrin, only two spectroscopic species were detected. An equilibrium model assuming a dendrimer-induced TSPP H-dimer coexisting with dendrimer-associated TSPP monomer afforded a good description of the experimental data, giving equilibrium constants (K_d) for the dimer dissociation of 0.78 and 2.67 for generations 2.0 and 4.0 dendrimers, respectively. The decomposition of the Soret band afforded TSPP H-aggregates' spectra with bandwidth values in the range 910−1210 cm^{-1}, clearly larger than the monomer bandwidth around 711−800 cm^{-1}. The fluorescence decays are nearly exponential with a long decay time component, which varies from 10 to 12 ns depending on the D/P ratio. However, at pH 2, there are striking differences between generations 2.0 and 4.0, which should be related to a more hydrophobic environment provided by the latter one. Time-resolved fluorescence anisotropy gave rotational times for the porphyrin−dendrimer complex from which hydrodynamic radii of approximately 14 and 21 Å, similar to those of generations 2.0 and 4.0 PAMAM dendrimers, were retrieved.

1. Introduction

Dendrimers are highly branched macromolecules that differentiate from other polymers due to their regular structure and well-defined topology.[1] These molecules are built around a core unit by adding covalently successive layers of monomer segments to the terminal points of the previous layer, usually designated as generations. Since each terminal point has a connecting multiplicity higher than one, the number of monomers in these structures grows exponentially with each generation. This feature is related to some of the unique characteristics of dendrimers, e.g., the maximum of intrinsic viscosity as a function of molar mass. Eventually a limit generation is reached, for which it is impossible to continue growing such structures due to stereochemical restraints.[2]

Although dendrimers' morphology depends significantly on their chemical structure, in general, the early generations present a more open and flexible structure, while the higher generations assume a globular conformation with a more compact structure, due to molecular packing.[3] In fact, dendrimers can be perceived as intermediates between polymers and colloids,[4] and that motivated studies on their interactions with other polymers.[5−10] In this respect, systems comprising charged dendrimers allowed testing theoretical models for the interaction of polyelectrolytes with oppositely charged particles.[5,6] Computer simulations using Monte Carlo methods have shown "reptilation" for the dendrimer's migration along the polyelectrolyte's chain.[10] In a different context, several studies on the binding ability of dendrimers to DNA molecules have been carried out.[8,9] Future applications of dendrimers as transfer vectors in gene therapy are being pursued.[11]

The polyelectrolyte character of dendrimers is usually related to their acid−base properties, and some attention has been given to proton and counterion binding on dendrimers.[12−15] In particular, a critical condition for nonspecific counterion condensation on spheres, analogous to the Manning condition, was proposed for carboxyl-terminated dendrimers.[13] The interaction of dendrimers with small ions has been used, from a different perspective, to study the structure and binding properties of dendrimers by the EPR technique.[16,17] The ability of dendrimers to bind metallic ions could be important for applications in the medical field, like radioimmunotherapy and imaging.[1,11,18]

Solvatochromic and fluorescence probes have been widely used in the study of dendrimers for their ability to report on the properties of surrounding media, like polarity and viscosity.[19−24] Fluorescence quenching of noncovalently dendrimer-associated dyes provides important information on the dynamics of reactions in restricted geometries.[25−28] Higher generation dendrimers can be considered as good model systems for testing theories on diffusion-controlled reactions at spherical surfaces, originally developed for micellar systems.[29,30] An analogy with micelles has already been suggested,[31] based on the similar size and shape of dendrimers and some spherical micelles and also the comparable values of micellar aggregation numbers and dendrimer's terminal groups. These similarities were further explored by functionalizing the dendrimer's outer shell with appropriate groups, e.g., alkyl chains, to clearly establish regions of different polarity.[1,3] However, dendrimers have different dynamic properties as compared to micelles, since they are unimolecular entities.

[†] Instituto Superior Técnico.
[‡] Katholieke Universiteit Leuven.
* Corresponding author: e-mail sbcosta@popsrv.ist.utl.pt.

10.1021/ma034844p CCC: $25.00
Published on Web 10/30/2003

The interaction of dendrimers with small probe molecules is also expected to report on the encapsulating properties of these systems, which could be of interest for their application as drug delivery agents.[32−36] The best-known example is probably Meijer's dendritic box,[32,33] where encapsulation of several Bengal rose molecules was carried out in poly(propylene imine) dendrimers functionalized with bulky amino acid derivatives as terminal groups. There are several examples in the literature of systems comprising dendrimers and porphyrin moieties.[37−40] However, only few of these focus on noncovalent interactions between porphyrins and dendrimers.[41,42] On the other hand, the potential application of porphyrins as building blocks in supramolecular assemblies has been revealed by several studies (e.g., involving the porphyrin focused in this work and polyelectrolytes,[43,44] surfactants,[45,46] and proteins[47]).

In a previous publication,[48] we report steady-state spectroscopic studies concerning the interaction of poly(amido amine) dendrimers (PAMAMs) of generations 2.0 and 4.0 with an ionic porphyrin, *meso*-tetrakis(4-sulfonatophenyl)porphine (TSPP). These studies showed that TSPP associates with PAMAMs, in aqueous media, to give several aggregated forms depending on dendrimer concentration and pH. For instance, in nonbuffered media and for dendrimer concentrations higher than the isoelectric point (of the charge balance between the porphyrin and dendrimer species) binding of TSPP to PAMAMs occurs with the formation of H-aggregates. On the other hand, at low pH, J-aggregation of TSPP occurs readily, and it seems to be enhanced in the dendrimer's presence. However, in this case significant differences between generations 2.0 and 4.0 PAMAMs were found, since the latter generation provides a more hydrophobic medium for the associated monomeric form of TSPP. This is in accordance with the more compact and densely packed structure assigned to PAMAM dendrimers from generation 3.0 onward.

In the present paper, we exploit these systems further and report a more quantitative study of their absorption spectra, supported by time-resolved fluorescence with picosecond resolution.

2. Experimental Section

Materials. PAMAM dendrimers of generations 2.0 and 4.0 were supplied by Aldrich as methanolic solutions with concentrations of 20 and 10 wt %, respectively. TSPP was acquired from Fluka with purum grade (>99%) and was used as received. Phosphate buffered saline was from Aldrich (catalog no. P-3813) and is supplied in individual foils as a preweighted mixture.

Samples were prepared with either bidistilled water or purified water from a Milli-Q Millipore system. For the systems studied at pH 2 Clark-Lubs' buffer was used. This buffer consists of an aqueous mixture of hydrochloric acid and potassium chloride with final concentrations of 10.6 and 50 mM, respectively. For the higher dendrimer concentrations studied a surplus of a concentrated HCl was added to compensate the basic character of these dendrimers. Other details concerning sample preparation have been given elsewhere.[48]

Apparatus. Steady-state absorption spectra were measured with a Jasco V-560 UV/vis spectrophotometer, and emission spectra were recorded in a Perkin-Elmer LS 50B spectrofluorimeter. The samples were thermostated at 298 K.

Fluorescence decays were obtained with a time-correlated single-photon counting (TCSPC) technique using two distinct equipments: an in-house assembled TCSPC setup, designated from here on as SPC setup, and a commercial equipment, Microtime 200, from Picoquant GmbH. A detailed description of the SPC setup is found elsewhere,[49] highlighting the flexibility of excitation wavelength tuning with this system. The excitation wavelengths of 420 and 488 nm (used with this setup) were generated with a flexible harmonic generator that gives the second and third harmonic of the titanium−sapphire laser fundamental. These wavelengths correspond to output powers of approximately 7 and 1.60 mW, respectively, for 420 and 488 nm. The repetition rate of the excitation laser was fixed at 8 MHz. Typical full widths at half-maximum obtained for this setup's instrument response function are in the order of a few tens of picoseconds.

Microtime 200 was originally developed for fluorescence lifetime imaging with microscopic samples using the TCSPC principle. In the present work, it was adapted for measuring solution samples in a cuvette by introducing an appropriate sample holder in the manual XY stage of the inverse microscope (Olympus IX 71). The measurements are performed in front-face geometry, and the backscattered light is attenuated through the use of appropriate filters. The excitation system consists of a pulse laser diode driver (PDL 800-B) equipped with two pulsed laser diodes heads for excitation at 400 and 635 nm (models LDH-P-C-400 and LDH-P-635, respectively). This unit allows the control of the repetition rate from 40 to 2.5 MHz (in powers of $^1/_2$) and the power level for the laser pulses. The maximum output powers for a repetition rate of 10 MHz are 0.4 and 1.4 mW for the 400 and 635 nm laser heads, respectively, while their minimum pulse widths are 54 and 83 ps. The detection system uses a photomultiplier tube from Picoquant (model PMA-182) with an instrument response time less than 250 ps. A band-pass filter with a transmission window in the range 670−740 nm and a long-pass filter that cuts wavelengths under 510 nm were used to eliminate backscattered light. Data acquisition is performed in a PC equipped with Timeharp 200 TCSPC board, also from Picoquant, which can record up to 4096 channels per range with a time increment smaller than 40 ps.

Data Analysis. The fluorescence decays were fitted with two analysis programs: TRFAGAP from Katholieke Universiteit Leuven and Fluofit version 3.1.0 from Picoquant. Both programs can be used to fit a multiexponential function (expression 1) through a nonlinear least-squares procedure based on the Marquardt−Levenberg algorithm[50] and combined with an iterative reconvolution method[51] to account for distortions of the decay signal from the instrument response function.

$$D(t) = \sum_{i=1}^{n} \alpha_i \exp(-t/\tau_i) \tag{1}$$

The quality of the fittings was judged by the usual statistical criteria and by visual inspection of the distribution of the weighed residuals and the autocorrelation function. In particular, the reduced χ^2 parameter, defined as

$$\chi^2 = \sum_i w_i (I_i - I(t_i))/\nu \tag{2}$$

should have a value close to one for a proper fit, where I_i is the decay intensity at channel i, $I(t_i)$ is the value of the fitted function at the same channel, w_i is the weighting factor, and ν is the number of degrees of freedom.

The relative importance of each component in the multiexponential fluorescence decays was evaluated from the decay time weighted preexponential factors F_i

$$F_i = \frac{\alpha_i \tau_i}{\sum_j \alpha_j \tau_j} \tag{3}$$

Whenever sufficient fluorescence decays at different detection wavelengths were collected, the decomposition of the decay

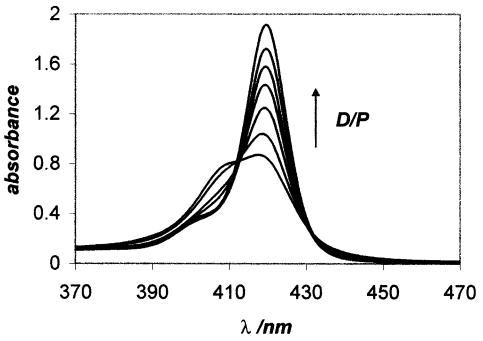

Figure 1. Absorption spectra of TSPP in the Soret band region for the systems with generation 4.0 PAMAMs (*D*/*P* ratio increases in the arrow's direction, taking the values 0.25, 0.5, 1, 2, 5, 10, and 100).

associated emission spectra ($DAS_i(\lambda)$) of the components contributing to the fluorescence decay was assessed:

$$DAS_i(\lambda) = \frac{\alpha_i \tau_i}{\sum_j \alpha_j \tau_j} I_{ss}(\lambda) = F_i I_{ss}(\lambda) \quad (4)$$

where $I_{ss}(\lambda)$ is the normalized intensity of emission from the steady-state spectra.

3. Results and Discussion

Steady-State Spectra. TSPP interacts with full generation PAMAM dendrimers to form several dendrimer-associated species depending on the relative concentration of dendrimer to porphyrin ($D/P \equiv$ [PAMAM]/[TSPP]), as it was concluded from a previous study using steady-state absorption and fluorescence techniques.[48] At low *D*/*P* ratios, the formation of large aggregates with low organization ("nonspecific aggregates") was proposed to explain the broad absorption spectrum, sometimes accompanied by turbidity, and the low emissivity of these systems. At *D*/*P* ratios above the isoelectric point of the charge balance between the dendrimer and porphyrin species, these systems reorganize to form TSPP H-aggregates, which gradually dissociate to yield the dendrimer-associated monomeric species with increasing dendrimer concentration. The position of the Soret band for the dendrimer-associated TSPP monomer, with the maximum at 419.5 nm, is reasonably shifted to the red in comparison to the free aqueous TSPP monomer, which has its maximum at 413 nm.

The results presented here report on such conditions that only dendrimer-induced TSPP H-aggregates and the dendrimer-associated monomeric species are present (Figure 1).

The formation of a well-defined isosbestic point around 412 nm suggests that these two species exist in equilibrium and justifies the application of a method based on the spectral variation to estimate the average number (n) of TSPP monomers in the H-aggregates.[52] This quantity is obtained from a plot of $\log(\theta(1 - \epsilon_\lambda/\epsilon_{\lambda,M}))$ vs $\log(\theta\epsilon_\lambda/\epsilon_{\lambda,M})$, where θ is the fraction of occupied sites in the dendrimer with porphyrin molecules, ϵ_λ is the average absorption coefficient at wavelength λ, and $\epsilon_{\lambda,M}$ is the absorption coefficient of the dendrimer-associated TSPP monomer at the same wavelength. The equilibrium constant of association was redefined in terms of the fraction θ when compared to the original version of the method, and the absorbance values were

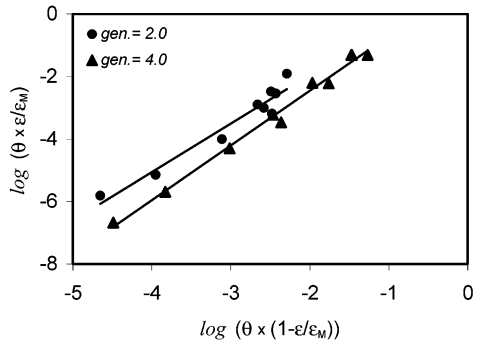

Figure 2. Plot of $\log(\theta(1 - \epsilon_\lambda/\epsilon_{\lambda,M}))$ vs $\log(\theta\epsilon_\lambda/\epsilon_{\lambda,M})$ for the systems with generation 2.0 (closed circles) and 4.0 (closed triangles) PAMAMs and linear regression plots for the same data.

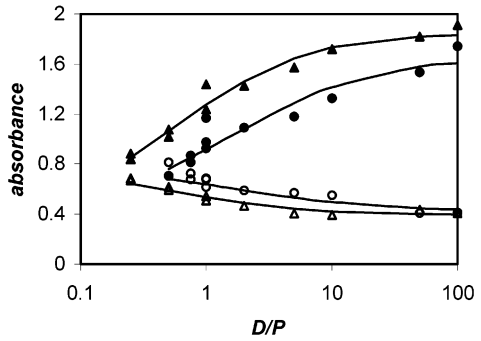

Figure 3. Absorbance variation with *D*/*P* ratio at the wavelengths of 405 nm (open symbols) and 420 nm (closed symbols) for the systems with generation 2.0 (circles) and 4.0 (triangles) PAMAMs. The lines were fitted using the monomer−dimer equilibrium model (see text for further details).

taken at 420 nm to ensure that the approximation $\epsilon_{\lambda,H}/n < \epsilon_\lambda$ is valid, where $\epsilon_{\lambda,H}$ is the absorption coefficient of the aggregated species. The slope gives an average aggregation number of 1.5 and 1.8 for generations 2.0 and 4.0, respectively (Figure 2).

The plot for generation 2.0 shows some curvature, which could mean that the distribution of aggregated forms in these systems does not follow a simple equilibrium: n (mon) ↔ agg, as it is assumed in this model. However, the results seem to indicate that the prevailing aggregated form should be the dimeric species for both generations studied, and a more specific model for monomer−dimer equilibrium was then applied:

$$P_2S + S \rightleftarrows 2PS, \quad K_d = \frac{[PS]^2}{[P_2S][S]} \quad (5)$$

In this case P_2S represents the dimer and S are the binding sites in the dendrimer, which should be proportional to the dendrimer concentration ($[S]_t = \alpha[PAMAM]$). Considering the spectral overlap of the Soret bands for the monomer (PS) and the H-aggregate (with maxima around 420 and 408 nm, respectively), the absorbance (Abs) at a given wavelength λ should be given by

$$Abs(\lambda) = \epsilon_{\lambda,H} l[P_2S] + \epsilon_{\lambda,M} l[PS] \quad (6)$$

where l is the optical length. A reasonable description of the experimental data was obtained (Figure 3), and from this the equilibrium constants (K_d) for dimer dissociation were retrieved, yielding values of 0.78 and 2.67 for generation 2.0 and 4.0 dendrimers, respectively.

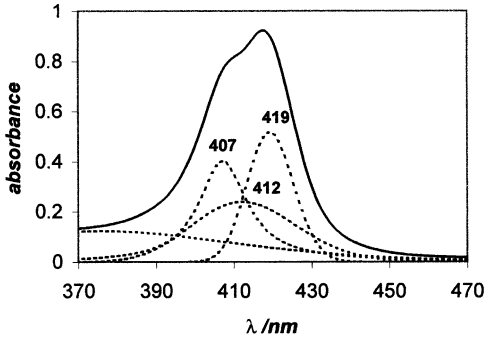

Figure 4. Decomposition of the Soret band for the system with generation 4.0 PAMAMs and $D/P = 0.25$, in the sum of Gaussian and Lorentzian functions (the respective maxima in nanometers are indicated in the figure, except for the broad Gaussian function that fits higher vibronic states in the short-wavelength region).

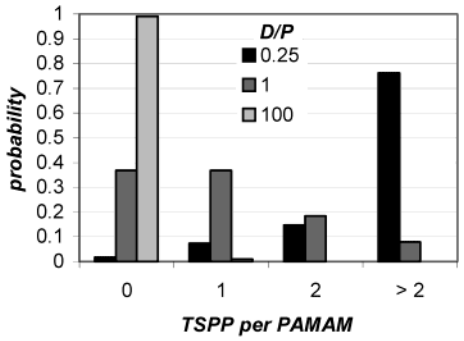

Figure 5. Probability associated with porphyrin occupancy number of PAMAM dendrimers estimated with Poisson's law.

Table 1. Decay Time Retrieved from Biexponential Fits of the Fluorescence Decays Measured for TSPP in Water (Nonbuffered Medium, 5 μM) with Excitation at 400, 420, and 635 nm

λ_{ex}/nm	λ_{em}/nm	F_1	τ_1/ns	F_2	τ_2/ns	χ^2
420[a]	630	0.998	10.28	0.002	1.01	1.176
	650	0.997		0.003		1.175
	670	0.993		0.007		1.096
	690	0.988		0.012		1.128
	710	0.988		0.012		1.161
	730	0.979		0.021		1.095
400[b]	670−740	0.995	10.00	0.005	0.283	1.106
635[b]	670−740	0.994	10.00	0.006	0.976	1.104

[a] Decays measured with the SPC setup. [b] Measured with Microtime 200.

In parallel, the decomposition of the absorption spectrum was attempted to obtain an independent estimate of the number of monomers in TSPP H-aggregates from the bandwidth of the respective Soret band. Theory predicts that the line shape of the exciton spectrum should scale with $N^{-1/2}$, with N being the coherence length of the exciton (or the number of monomers effectively coupled), due to an exchange narrowing mechanism that averages local inhomogeneities throughout the aggregate.[53,54] However, intersite correlation resulting from structural disorder of the aggregate or from strong exciton−phonon interaction can lead to weaker dependencies of the aggregate bandwidth with N.

The Soret band of dendrimer-associated TSPP monomer is fairly described with two Gaussian functions, while the aggregate band is better fitted with a Lorentzian function (Figure 4). An additional Gaussian was required to account for higher vibronic states.

The fact that the aggregate band is approximately Lorentzian agrees with theoretical studies. In particular, for H-aggregates, which have a positive intermolecular coupling ($V > 0$), the spectrum should exhibit a broader wing toward the low-energy side due to transitions to in-band states, which are "weakly" allowed in a linear aggregate geometry.[53,54]

The values fitted for the bandwidth of TSPP H-aggregates spectra are in the range 910−1210 cm^{-1}, which surpass the bandwidth values for the monomeric species that are around 711−800 cm^{-1}. This probably means that in these aggregates the exciton delocalization that should lead to exchange narrowing of the line shape is not effective enough when compared to other mechanisms of inhomogeneous line broadening. On the other hand, it is also possible that the decomposition procedure fails to properly separate the several components of the absorption spectrum due to the severe overlap of the individual bands (Figures 1 and 4) or due to a poor description of the asymmetric aggregates' line shape.

In the absence of other supporting evidence, it may be simplistic to claim that the TSPP aggregated form in these systems is the dimer. As was previously mentioned,[48] it is likely that a statistical distribution of aggregate stoichiometries exists. Using Poisson law to describe TSPP's distribution among the dendrimers, in analogy with micellar media,[24,26,27] it is possible to estimate that the probability of finding more than two porphyrins per dendrimer for the lower D/P ratio used in the plot of Figure 1 is as high as 76%, and even for a D/P ratio of one this probability is still 8% (Figure 5).

So statistically there is a considerable probability that aggregates higher than the dimer are formed, although no significant deviations to the monomer−dimer model applied to spectral variations were observed. On the other hand, it is remarkable that the aggregate's Soret band presents similar characteristics for both generations 2.0 and 4.0. Assuming that these are "dendrimer-templated" aggregates, the dendrimer's conformation, which depends significantly on the generation,[21,55] should have some effect in the aggregate's structure and/or dimension, which would result in different coherence lengths and therefore in changes of the electronic spectrum with dendrimer generation. Molecular dynamics studies currently being undertaken are expected to shed some light regarding this issue.

Time-Resolved Fluorescence. *TSPP in Aqueous Solution.* Prior to presenting the results for the systems with TSPP and PAMAM dendrimers, the fluorescence decay time behavior of TSPP alone in water will be reviewed, since this information will be useful in the comprehension of the results obtained in dendrimers' presence.

The fluorescence decays measured for an aqueous solution of TSPP with 5 μM concentration using the SPC setup are almost single exponential with a major lifetime component of 10.3 ns (Table 1). However, a second component with a decay time of about 1 ns and a residual weight of less than 2% is required to properly fit these decays.

Other authors[56,57] reported slightly lower values, of about 9.3−9.5 ns, for the major lifetime component of TSPP fluorescence decay in water, but these values were obtained at higher TSPP concentrations, in the range 10−50 μM. Van Patten et al.,[43] who worked with concentrations of TSPP on the order of 10^{-7} M, report

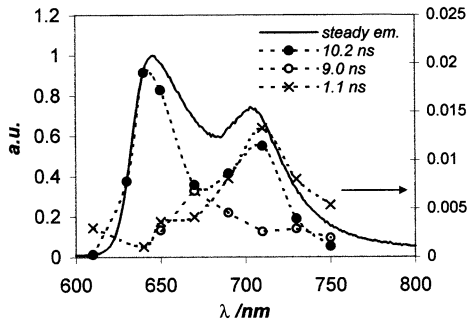

Figure 6. Emission spectra (solid line) and weighed preexponentials for the decay time components of 10.2 ns (close circles and thin line), 9.0 ns (open circles and dashed line), and 1.1 ns (crosses and dashed/dotted line) fitted from a global analysis of the fluorescence decays obtained for TSPP in PBS medium (excitation at 420 nm).

a lifetime value of 10.2 ns for TSPP, which better agrees with our results. These authors also mention that "reduced lifetimes with multiexponential (decay) kinetics" were obtained for aged samples with concentrations of less than 10 μM. The sample's pH is also referred as an important parameter, since this compound has a pK_a of 4.8 units and its diacid form exhibits a significantly lower fluorescence lifetime of about 3.9 ns. To circumvent this issue, some measurements were performed in buffered medium using phosphate buffered saline (PBS), which has a pH of 7.4 units. However, under these conditions, the decays' complexity increases, and it is not possible to perform a global analysis with a biexponential law, since the major decay time slightly decreases from 10.3 to 9.5 ns as the detection wavelength is shifted toward the red edge of the emission spectrum. The steady-state absorption spectrum of TSPP in buffered medium also shows some differences in comparison to that of TSPP in water (data not shown). The maximum of the Soret decreases slightly, and the bandwidth increases. A tail appears in the red edge of the Q bands in the absorption and emission spectra. Similar features have been previously identified and were attributed to the aggregation of this porphyrin, most probably to form a mixture of H- and J-dimers.[56] In the present case, the aggregation of TSPP would be induced by the increased ionic strength of the buffered media. A global analysis of the decays measured for the different detection wavelengths required four exponential components. The decay associated emission spectra (DAS$_i(\lambda)$) were calculated according to expression 4 and are depicted in Figure 6 for the three major components.

The lifetime of monomeric TSPP in water (10.2 ns) is the dominant component throughout the emission spectra. Another decay time component has a value close to 9.0 ns and a relative weight that shows two ill-defined maxima like the emission spectra (similar to the vibronic structure of Q(0,0) and Q(0,1)), but shifted to the red. It can be attributed to a loosely aggregated form, since in this case the weak electronic coupling is not expected to affect significantly the radiative dynamics of the species involved (that would explain the absence of a well-defined shift in the absorption bands' position).

TSPP−PAMAMs in Aqueous Media (Nonbuffered). The fluorescence decay times of TSPP in the systems with PAMAM dendrimers—*D*/*P* ratios of 1, 10, and 100—measured with the SPC setup are presented in Table 2.

Table 2. Fluorescence Decay Times of TSPP in the Systems with PAMAM Dendrimers of Generations (Gen) 2.0 and 4.0 (Nonbuffered Media)[a]

	D/*P*	λ_{em}/nm	F_1	τ_1/ns	F_2	τ_2/ns	χ^2
gen = 2.0	1	650	0.993	11.60	0.007	0.995	1.144
		710	0.992		0.008		1.110
	10	650	0.995	11.94	0.005	0.897	1.113
		710	0.995		0.005		1.033
	100	650	0.996	12.01	0.004	0.816	1.125
		710	0.995		0.005		1.073
gen = 4.0	1	650	0.991	11.82	0.009	1.11	1.080
		710	0.991		0.009		1.086
	10	650	0.996	11.99	0.004	0.834	1.100
		710	0.995		0.005		1.143
	100	650	0.996	12.08	0.004	0.942	1.065
		710	0.995		0.005		1.096

[a] The fluorescence decays were measured with excitation at 420 nm and detection at 650 and 710 nm and then globally analyzed for each *D*/*P* ratio.

These decays were obtained with excitation at 420 nm corresponding to the region of maximum absorbance of the monomeric form of dendrimer-associated TSPP (Figure 7a).

Two components were retrieved from fitting the decay curves with a multiexponential law: a major component with a decay time in the range of 11−12 ns that slightly increases with dendrimer concentration and a second component with a weight inferior to 1% and a decay time around 1 ns. This latter component is probably due to a small fraction of the aggregated form that still absorbs at this wavelength. This was confirmed from the excitation spectra (data not shown) recovered at 680 nm (where the emission from the aggregated form is more significant, relative to the monomer), which exhibit a band centered around 410 nm with broad wings that extend as far as 480 nm in the red edge. Unfortunately, the emission spectrum of the aggregated form largely overlaps that of the monomeric form, which makes it impossible to completely resolve their respective components.

The fluorescence decay times of these systems were also measured in the Microtime 200 equipment with excitation at 400 nm and detection in the interval 670−740 nm (Figure 7b). Biexponential decays were also obtained in this case, as it is presented in Table 3 for the systems with generation 2.0 dendrimers.

However, the main decay time component presents slightly lower values in the range 10.5−11.5 ns but maintains the increasing trend with dendrimer concentration. On the other hand, the short decay time increases to values around 2−3 ns, and its respective weight also increases to 1−2% with excitation at 400 nm. There seems to be no direct relation between this short component and the species responsible for the absorption band around 408 nm (dendrimer-induced TSPP H-aggregates), since no significant increase in this component's relative weight is observed with excitation at 400 nm. Most probably, this component has its origin in smaller or less organized aggregates, and it reflects a distribution of lifetimes arising from the polydispersity of these aggregates, which would explain the small discrepancies found for different excitation/detection conditions.

The absence of a specific lifetime component for the dendrimer-induced H-aggregates would be easily explained considering the low emissivity of this type of aggregate. However, this contradicts the results from excitation spectra (data not shown), which show a

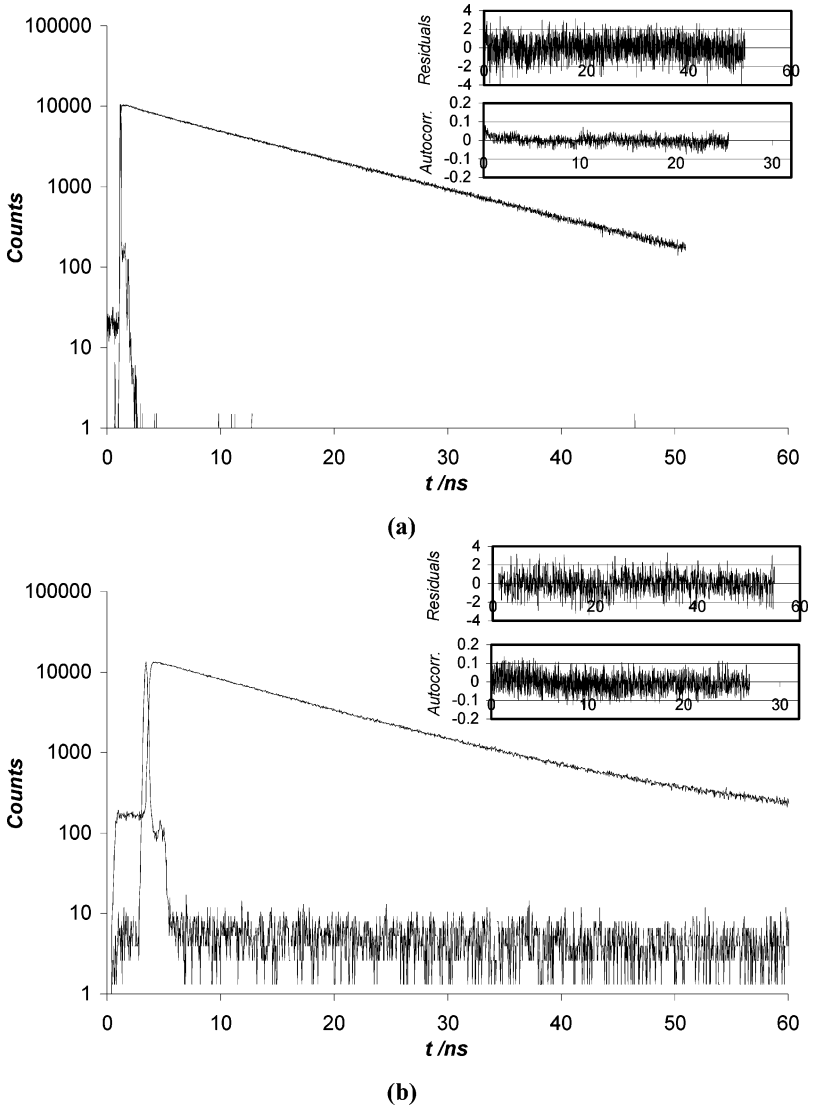

Figure 7. Examples of fluorescence decays obtained for TSPP with PAMAM dendrimers of generation 4.0 ($D/P = 1$) using the SPC setup with excitation at 420 nm and detection at 650 nm (a) and using Microtime 200 with excitation at 400 nm and detection in the range 670−740 nm (b). The residuals and autocorrelation plots for a biexponential analysis are shown in the insets.

Table 3. Fluorescence Decay Times of TSPP in the Systems with PAMAM Dendrimers (Nonbuffered Media)[a]

	D/P	F_1	τ_1/ns	F_2	τ_2/ns	χ^2
gen = 2.0	0.75	0.984	10.49	0.016	2.89	1.078
	1	0.990	10.50	0.010	2.05	1.013
	2	0.982	10.80	0.018	2.93	1.107
	5	0.985	11.00	0.015	2.51	1.085
	50	0.983	11.37	0.017	2.08	1.074
gen = 4.0	0.25	0.981	10.95	0.019	4.15	1.079
	0.5	0.991	11.05	0.009	4.67	1.078
	1	0.984	11.18	0.016	4.90	1.175
	2	0.978	11.28	0.022	4.46	1.211
	5	0.973	11.30	0.027	4.49	1.140
	50	0.953	11.64	0.047	5.22	1.096

[a] The fluorescence decays were measured in Microtime 200 FLIM equipment with excitation at 400 and detection in the range 670−740 nm using a band-pass filter.

prominent band with a maximum around 410 nm that reasonably reproduces the absorption band attributed to TSPP H-aggregates. In this case an alternative explanation invoking the electronic structure of porphyrins seems more adequate. The four orbital model of Gouterman[58] describes the visible and near-UV spectrum of porphyrins on the basis of a configuration interaction that mixes the electronic configurations $^1(a_{2u}e_g)$ and $^1(a_{1u}e_g)$ and gives rise to the couple of strong and weakly allowed B and Q transitions, respectively. Since classical exciton theory[59,60] predicts that electronic coupling is proportional to the transition dipole moment, the effect in the absorption spectrum is more pronounced for the B or Soret band of aggregated TSPP, and a well-defined blue shift is observed in this case. In contrast, the set of Q bands shift in the opposite direction, which seems contradictory. Probably the excitonic coupling for this transition is not strong enough to overcome the stabilization effect of π, π interactions between the porphyrin rings in the aggregate, and a red shift is observed instead. The weak electronic coupling in the Q bands, which correspond to the emitting state, precludes any effects in the emission dynamics, like superradiance.[61−63] Unless some nonradiative deactivation mode is enhanced in the H-aggregates, it is reasonable to assume that its lifetime is very close to that of the monomeric species, and therefore these are not distinguished in the fluorescence decays. The observed trend in the long decay time component, with dendrimer concentration, would then be explained by the gradual disruption of TSPP H-

Table 4. Fluorescence Decay Times of TSPP at pH 2 in Aqueous Media and with PAMAM Dendrimers of Generations (Gen) 2.0 and 4.0[a]

	D/*P*	λ_{ex}/nm	λ_{em}/nm	F_1	τ_1/ns	F_2	τ_2/ns	F_3	τ_3/ns	χ^2
TSPP (pH 2)		420	640	0.999	3.86	0.001	0.236			1.283
			675	0.995		0.005				1.173
		488	640	0.989	3.88	0.006	0.424	0.005	0.045	1.059
			675	0.984		0.009		0.007		1.144
gen = 2.0	100	420	675	0.660	4.20	0.332	2.59	0.008	0.228	0.964
gen = 4.0	100	420	650	0.926	11.07	0.072	2.54	0.002	0.221	1.034

[a] The decays obtained for several detection wavelengths were globally analyzed with linked decay times.

Table 5. Fluorescence Decay Times of TSPP at pH 2 in Aqueous Media and with PAMAM Dendrimers of Generations (Gen) 2.0 and 4.0 Measured in Microtime 200 Equipment

	D/*P*	λ_{ex}/nm	λ_{em}/nm	F_1	τ_1/ns	F_2	τ_2/ns	F_3	τ_3/ns	F_4	τ_4/ns	χ^2
TSPP (pH 2)		400	510	1.000	3.64							1.045
		635	670−740	0.991	3.69	0.009	0.079					1.036
gen = 2.0	50	400	510	0.635	6.64	0.257	2.02	0.070	0.342	0.038	0.052	1.088
	100	400	510	0.683	6.72	0.229	1.93	0.064	0.315	0.024	0.038	0.928
	100	635	670−740	0.108	5.24	0.850	3.25			0.042	0.092	1.053
gen = 4.0	50	400	510	0.743	9.34	0.200	2.44	0.040	0.371	0.017	0.071	1.035
	100	400	510	0.591	9.11	0.332	2.51	0.077	0.252			1.107
	100	635	670−740	0.032	9.45	0.939	2.77	0.028	0.273			1.106

aggregates to yield the dendrimer-associated monomeric species that presents a slightly longer lifetime in the hydrophobic environment of the dendrimer.

The fluorescence decay times obtained for the systems with generation 4.0 dendrimers using Microtime 200 equipment are presented in Table 3. Some differences are observed when compared with the results for generation 2.0 and those from the SPC setup. In particular, with excitation at 400 nm the short decay time component increases to a value around 4−5 ns, but its relative weight remains low (inferior to 5%). However, it is possible to adjust the same decays with a short component fixed at 2 ns and still obtain satisfactory quality parameters for the fittings. In fact, these decays deviate so slightly from single exponentiality that it is difficult to retrieve the short decay time with accuracy, and a set of solutions exists for which this component varies in the range 2−8 ns without affecting the χ^2 more than 1% (asymptotic standard error analysis performed with FluoFit).

TSPP−PAMAMs at Low pH. The fluorescence decays of TSPP in these systems were also obtained at pH 2. In these conditions TSPP readily forms J-aggregates that are detected in the UV/vis spectrum as two bands centered at 490 and 704 nm, which correspond to the red-shifted Soret and Q bands of the J-aggregate, respectively. This type of aggregation has been extensively studied for TSPP,[45,46,56,57,64−67] and in particular, time-resolved absorption and fluorescence studies with femtosecond resolution have already been carried out.[68−70] The fluorescence decay times obtained for TSPP in water at pH 2 are given in Table 4 and Table 5 for the measurements performed with the SPC setup and the Microtime 200 equipment, respectively.

In general, the results agree with the values reported in the literature for the lifetime of diacid TSPP, which are in the range 3.5−3.9 ns, and of its J-aggregate, in which case two components with approximate values of 300 and 50 ps have been identified by phase modulation[57] and single photon counting.[56] However, in the present work a component of 45 ps was found with excitation at 488 nm, in the J-aggregate's Soret band, which in previous studies was detected only for direct excitation of the J-aggregate's Q bands, in contrast with the 300 ps component that is present in both cases. This was explained by Akins et al.[57] invoking differences in exciton coherence length between direct excitation of the emitting state or vibrational relaxation from a higher electronic state. Since the emission spectrum of the diacid form overlaps the Q bands of the J-aggregate, it is possible that this state is directly populated by a mechanism of radiative energy transfer, and this would enable the detection of its decay time component in these conditions.

The fluorescence decays for the systems with PAMAM dendrimers at pH 2 were measured only for high *D*/*P* ratios, since phase separation occurred for low dendrimer concentrations.[48] The decays obtained for a *D*/*P* ratio of 100 with the SPC setup were fitted with three exponential components (Table 4). The shorter components with decay times around 2.5 ns and 220 ps are common for both generations studied and can be attributed to the diacid form of TSPP and its J-aggregate, respectively. On the other hand, the major decay time component presents a value of 11.1 ns for generation 4.0, resembling the values obtained for the same systems at high pH, while for generation 2.0 this component has a value of 4.2 ns, close to the lifetime of diacid TSPP in water. This difference was interpreted according to a more compact structure of generation 4.0 dendrimers, which provides a more hydrophobic environment for the encapsulated TSPP molecules. Molecular dynamics studies[55]—later experimentally confirmed[19,21,24−27,31,71]—showed that PAMAM dendrimers undergo a morphological transition around generation 3 from an open and oblate conformation to a more compact and spherical one, which prevails at higher generations. Although no evidence was found in the steady-state absorption spectrum for the presence of TSPP's deprotonated form, this seems a reasonable explanation for the long decay time observed in the systems with generation 4.0 PAMAMs. In fact, studies on the interaction of TSPP with human serum albumin[47] (HSA) revealed a lifting of the Q bands degeneracy at pH 2 and a fluorescence decay time of 12.9 ns (with a residual component of 3.8 ns) for TSPP in the protein's presence. On the other hand, the same study showed that, although no lifting of the Q bands degeneracy occurs for the interaction of TSPP with β-lactoglobulin (β-LG) at pH 2, the fluorescence decays present

Table 6. Initial Anisotropy (r_0) and Rotational Decay Times (ϕ) Obtained from Time-Resolved Fluorescence Anisotropy for TSPP in Aqueous Media and with PAMAM Dendrimers of Generations (Gen) 2.0 and 4.0 (Excitation at 420 nm)

	D/*P*	λ_{em}/nm	r_0	ϕ/ns	χ^2
TSPP(aq)	0	650	0.058	0.377	1.123
gen = 2.0	1	650	0.032	2.31	1.071
	10	650	0.029	2.39	1.074
	100	650	0.027	2.80	1.103
gen = 4.0	1	650	0.027	8.02	1.084
	10	650, 710	0.032	8.84	1.197
	100	650, 710	0.033	9.05	1.149
pH 2	100	650	0.024	5.40	1.096

a minor component with a decay time around 13 ns. This was interpreted according to a more hydrophobic location of TSPP within HSA in comparison to β-LG. Similar phenomenology was also observed for the interaction of TSPP with the surfactants cetyltrimethylammonium bromide and Triton X-100 at low pH.[45]

The fluorescence decays measured for TSPP in the presence of PAMAM dendrimers at pH 2 with Microtime 200 equipment show slight differences (Table 5), although overall the results agree with those from the SPC setup.

Time-Resolved Fluorescence Anisotropy. Time-resolved anisotropy was obtained for the systems studied from the respective fluorescence decays measured with detection at several polarization angles: 0°, 90°, and 54.7° (magic angle), while keeping the excitation polarization angle perpendicular to the excitation-detection plane. The decays were adjusted following the method of global analysis of unmatched polarized fluorescence decay curves,[72] which circumvents any artifacts from arithmetic manipulation of decay curves by directly fitting each polarized decay weighted with an appropriate matching factor.

$$I_i(\theta,t) = [\kappa(\theta)/3]\sum_j \alpha_j \exp(-t/\tau_j)[1 + (3\cos^2\theta - 1) \times (r_\infty + \sum_k L_{jk}\beta_k \exp(-t/\phi_k))] \quad (7)$$

where I_i is the intensity of the fluorescence decay at instant t and for detection at θ polarization angle, κ is the matching factor, and L_{jk} are the elements of the association matrix L between the decay time components τ_j and the rotational decay times ϕ_k (see ref 72 for further details). Another advantage of this method is that it does not require the determination of the G factor for the experimental setup, although it requires at least three fluorescence decays obtained for different detection polarization angles, which can be different from the parallel and perpendicular polarized decays used in the "classic" method.

The anisotropy trace obtained for TSPP alone in water is single exponential with an initial anisotropy, r_0, of 0.058 and a rotational lifetime of 377 ps (Table 6).

This value agrees well with the rotational lifetime of 410 ps reported by Maiti et al.,[56] although these authors give a higher value for the initial anisotropy of 0.32 and a value of 0.018 for the steady-state anisotropy. In the present analysis, the steady-state anisotropy, r_∞, was fixed to zero, since the rotational freedom of this molecule in aqueous solution allows for complete depolarization at sufficiently long times, which was confirmed by steady-state fluorescence anisotropy. On the other hand, the limiting anisotropy r_0 is defined as[73]

$$r_0 = 0.4\left(\frac{3\cos^2\alpha - 1}{2}\right) \quad (8)$$

where α is the angle between absorption and emission dipoles. The positive value obtained for r_0 means that α is smaller than the magic angle (54.7°). Since TSPP is a free base porphyrin at neutral pH, the transition moment of B (excited S_2 state) and Q bands (emitting S_1 state) is split into two components, *x* and *y*, with polarization in the porphyrin plane and parallel/perpendicular orientations regarding the pyrrole N−H axis, respectively.[58] Even though the emitting Q state is the *x*-polarized, the B states overlap considerably, and probably these are simultaneously excited, making it difficult to qualitatively predict the relative polarization of the absorption dipole. Besides that, depolarization could also occur in the relaxation process from S_2 to S_1 state.

In the presence of PAMAM dendrimers the anisotropy traces remain single exponential, although the respective rotational decay times increase about 6 and 21 times for generation 2.0 and 4.0, respectively. A slight increase is also observed with increasing *D*/*P* ratio between 1 and 100. A possible interpretation for these results would be to attribute the increase in the rotational decay times to a higher viscosity experienced by TSPP in the dendrimer "environment" that would equally affect the monomeric and the H-aggregated forms present in this *D*/*P* range. On the other hand, the nonspecific aggregates represent only a small fraction of the TSPP population to significantly affect the fluorescence anisotropy decay. However, the increase in the rotational decay times of dendrimer-associated TSPP could also be ascribed to a simultaneous rotation of TSPP and the dendrimer, as a whole. In this case, the Stokes−Debye−Einstein (SDE) equation can be used to estimate the radius of this porphyrin−dendrimer complex, under the premise that this entity behaves like a spherical rotor.

$$\phi = \frac{\eta V C f}{kT} \quad (9)$$

Sticking boundary conditions, $C = 1$, were assumed since the dendrimers' size is much larger than the solvent molecules and the Perrin factor, *f*, was disregarded in a first approach. The value used for the viscosity of water at 25 °C was 0.89 mPa s.[74] This gave radius estimates in the range 13.7−14.6 Å for the porphyrin−dendrimer complex with generation 2.0 and in the range 20.7−21.5 Å for generation 4.0. These values closely agree with the radius of 14.5 and 22.5 Å given for PAMAM dendrimers of generations 2.0 and 4.0,[75] respectively, supporting the assumption that TSPP is strongly associated with the dendrimers and that these species rotate together. The increase of the rotational decay times with dendrimer concentration could be explained with a concomitant increase in the medium's viscosity, which was not taken into account in the estimates carried out.

Time-resolved fluorescence anisotropy for TSPP in the presence of PAMAM dendrimers at pH 2 was only measured for generation 4.0 and a D/P ratio of 100 (Table 5). A lower rotational decay time of 5.4 ns was retrieved for this system, which seems contradictory

with the increase predicted for the radius of these dendrimers at low pH.[76,77] The complexity of the fluorescence decay contrasts with the single-exponential decay obtained for the anisotropy, which could mean that the rotational decay time retrieved is, in fact, an averaged lifetime for the different fluorescence components. Other mechanisms of depolarization may occur in this system. In particular, the J-aggregates present in this system could be responsible for an increase in the fluorescence depolarization rate through a mechanism of energy transfer,[56] although some care should be taken in discussing the time scales involved.

4. Concluding Remarks

Dendrimer−porphyrin assemblies were studied at high *D*/*P* ratios for generations 2.0 and 4.0, where dendrimer-associated monomeric TSPP and its H-aggregates coexist in equilibrium. Attempts to determine the H-aggregates' stoichiometry from steady-state absorption measurements indicate that the dimer is the prevailing species. Time-resolved fluorescence studies afforded two decay time components: a long one in the range 10−12 ns and a short one with a few nanoseconds and a relative weight inferior to 5%. The latter was attributed to nonspecific aggregates of TSPP, since similar decay times were already observed in the absence of PAMAM dendrimers. The long decay time component increases slightly with dendrimer concentration, which was attributed to a gradual disruption of the dendrimer-induced TSPP H-aggregates to give the monomeric form. Identical lifetimes were assumed for these two species on the basis of weak electronic coupling for the emitting state in the aggregate. No significant differences were observed between generations 2.0 and 4.0, except that dissociation of TSPP H-aggregates occurs more efficiently for the higher generation. On the other hand, at low pH the fluorescence decays of TSPP in these systems show a long component for generation 4.0, with a decay time close to that of the dendrimer-associated TSPP monomer, which was not detected for generation 2.0. This was assigned to a more hydrophobic environment of TSPP in the higher generation PAMAM dendrimers, in accordance with a structural transition, from an open and discoid conformation to a more compact and spherical one, established for these dendrimers around generation 3.

Time-resolved fluorescence anisotropy measurements enable the recovery of the hydrodynamic radius of a porphyrin−dendrimer complex from the rotational decay times obtained for these systems. A close agreement with the values known for the dendrimers radius supports a strong association between TSPP and PAMAM dendrimers.

Acknowledgment. This work was supported by CQE IV, Project POCTI/QUI/35398/2000. P. M. Paulo acknowledges a Ph.D. Grant BD 21698/99 from Praxis XXI-FCT. The European Science Foundation is also gratefully acknowledged for financial support of a short-term visit to the Laboratory for Molecular Dynamics and Spectroscopy, Department of Chemistry, Katholieke Universiteit Leuven−Belgium, under the ULTRA Programme on Femtochemistry and Femtobiology. Partial support by Fundação Calouste Gulbenkian is also gratefully acknowledged.

References and Notes

(1) Bosman, A. W.; Janssen, H. M.; Meijer, E. W. *Chem. Rev.* **1999**, *99*, 1665−1688.
(2) de Gennes, P. G.; Hervet, H. J. *J. Phys. (Paris)* **1983**, *44*, L351−L360.
(3) Tomalia, D. A.; Naylor, A. M.; Goddard, W. A., III *Angew. Chem., Int. Ed. Engl.* **1990**, *29*, 138−175.
(4) Likos, C. N.; Schmidt, M.; Löwen, H.; Ballauf, M.; Pötschke, D.; Lindner, P. *Macromolecules* **2001**, *34*, 2914−2920.
(5) Zhang, H.; Dublin, P. L.; Ray, J.; Manning, G. S.; Moorefield, C. N.; Newkome, G. R. *J. Phys. Chem. B* **1999**, *103*, 2347−2354.
(6) Miura, N.; Dublin, P. L.; Moorefield, C. N.; Newkome, G. R. *Langmuir* **1999**, *15*, 4245−4250.
(7) Tsutsumiuchi, K.; Aoi, K.; Okada, M. *Polym. J.* **2000**, *32*, 107−112.
(8) Kabanov, V. A.; Sergeyev, V. G.; Pyshkina, O. A.; Zinchenko, A. A.; Zezin, A. B.; Joosten, J. G. H.; Brackman, J.; Yoshikawa, K. *Macromolecules* **2000**, *33*, 9587−9593.
(9) Ottaviani, M. F.; Furini, F.; Casini, A.; Turro, N. J.; Jockusch, S.; Tomalia, D. A.; Messori, L. *Macromolecules* **2000**, *33*, 7842−7851.
(10) Welch, P.; Muthukumar, M. *Macromolecules* **2000**, *33*, 6159−6167.
(11) Zeng, F.; Zimmerman, S. C. *Chem. Rev.* **1997**, *97*, 1681−1712.
(12) Borkovec, M.; Koper, G. J. M. *Macromolecules* **1997**, *30*, 2151−2158.
(13) Huang, Q. R.; Dublin, P. L.; Moorefield, C. N.; Newkome, G. R. *J. Phys. Chem. B* **2000**, *104*, 898−904.
(14) van Duijvenbode, R. C.; Rajanayagam, A.; Koper, G. J. M.; Baars, M. W. P. L.; de Waal, B. F. M.; Meijer, E. W.; Borkovec, M. *Macromolecules* **2000**, *33*, 46−52.
(15) Sun, L.; Crooks, R. M. *J. Phys. Chem. B* **2002**, *106*, 5864−5872.
(16) Ottaviani, M. F.; Bossmann, S. H.; Turro, N. J.; Tomalia, D. A. *J. Am. Chem. Soc.* **1994**, *116*, 661−671.
(17) Ottaviani, M. F.; Montalti, F.; Romanelli, M.; Turro, N. J.; Tomalia, D. A. *J. Phys. Chem.* **1996**, *100*, 11033−11042.
(18) Wu, C.; Brechbiel, M. W.; Kozak, R. W.; Gansow, O. A. *Bioorg. Med. Chem. Lett.* **1994**, *4*, 449−454.
(19) Jockush, S.; Turro, N. J.; Tomalia, D. A. *Macromolecules* **1995**, *28*, 7416−7418.
(20) Pistolis, G.; Malliaris, A.; Paleos, C. M.; Tsiourvas, D. *Langmuir* **1997**, *13*, 5870−5875.
(21) Jockush, S.; Ramirez, J.; Sanghvi, K.; Nociti, R.; Turro, N. J.; Tomalia, D. A. *Macromolecules* **1999**, *32*, 4419−4423.
(22) Wade, D. A.; Torres, P. A.; Tucker, S. A. *Anal. Chim. Acta* **1999**, *397*, 17−31.
(23) Richter-Egger, D. L.; Li, H.; Tucker, S. A. *Appl. Spectrosc.* **2000**, *54*, 1151−1156.
(24) Richter-Egger, D. L.; Landry, J. C.; Tesfai, A.; Tucker, S. A. *J. Phys. Chem. A* **2001**, *105*, 6826−6833.
(25) Moreno-Bondi, M. C.; Orellana, G.; Turro, N. J.; Tomalia, D. A. *Macromolecules* **1990**, *23*, 910−912.
(26) Turro, C.; Niu, S.; Bossmann, S. H.; Tomalia, D. A.; Turro, N. J. *J. Phys. Chem.* **1995**, *99*, 5512−5517.
(27) ben-Avraham, D.; Schulman, L. S.; Bossmann, S. H.; Turro, C.; Turro, N. J. *J. Phys. Chem. B* **1998**, *102*, 5088−5093.
(28) Kleinman, M. H.; Flory, J. H.; Tomalia, D. A.; Turro, N. J. *J. Phys. Chem. B* **2000**, *104*, 11472−11479.
(29) Van der Auweraer, M.; Dederen, J. C.; Geladé, E.; De Schryver, F. C. *J. Chem. Phys.* **1981**, *74*, 1140−1147.
(30) Sano, H.; Tachiya, M. *J. Chem. Phys.* **1981**, *75*, 2870−2878.
(31) Gopidas, K. R.; Leheny, A. R.; Caminati, G.; Turro, N. J.; Tomalia, D. A. *J. Am. Chem. Soc.* **1991**, *113*, 7335−7342.
(32) Jansen, J. F. G. A.; de Brabander-van den Berg, E. M. M.; Meijer, E. W. *Science* **1994**, *266*, 1226−1229.
(33) Miklis, P.; Çain, T.; Goddard, W. A., III *J. Am. Chem. Soc.* **1997**, *119*, 7458−7462.
(34) Sideratou, Z.; Tsiourvas, D.; Paleos, C. M. *Langmuir* **2000**, *16*, 1766−1769.
(35) Köhn, F.; Hofkens, J.; Wiesler, U.-M.; Cotlet, M.; van der Auweraer, M.; Müllen, K.; De Schryver, F. C. *Chem.−Eur. J.* **2001**, *7*, 4126−4133.
(36) Köhn, F.; Hofkens, J.; Gronheid, R.; Cotlet, M.; Müllen, K.; Van der Auweraer, M.; De Schryver, F. C. *Chem. Phys. Chem.* **2002**, *110*, 985−1072.
(37) Matos, M. S.; Hofkens, J.; Verheijen, W.; De Schryver, F. C.; Hecht, S.; Pollak, K. W.; Fréchet, J. M. J.; Forier, B.; Dehaen, W. *Macromolecules* **2000**, *33*, 2967−2973.
(38) Jiang, D.-L.; Aida, T. *J. Am. Chem. Soc.* **1998**, *120*, 10895−10901.

(39) Stapert, H. R.; Nishiyama, N.; Jiang, D.-L.; Aida, T.; Kataoka, K. *Langmuir* **2000**, *16*, 8182−8188.
(40) Rajesh, C. S.; Capitosti, G. J.; Cramer, S. J.; Modarelli, D. A. *J. Phys. Chem. B* **2001**, *105*, 10175−10188.
(41) Bo, Z.; Zhang, L.; Wang, Z.; Zhang, X.; Shen, J. *Mater. Sci. Eng., C* **1999**, *10*, 165−170.
(42) Sakamoto, M.; Ueno, A.; Mihara, H. *Chem.—Eur. J.* **2001**, *7*, 2449−2458.
(43) Van Patten, P. G.; Shreve, A. P.; Donohoe, R. J. *J. Phys. Chem. B* **2000**, *104*, 5986−5992.
(44) Purrello, R.; Raudino, A.; Scolaro, L. M.; Loisi, A.; Bellacchio, E.; Lauceri, R. *J. Phys. Chem. B* **2000**, *104*, 10900−10908.
(45) Maiti, N. C.; Mazumdar, S.; Periasamy, N. *J. Phys. Chem. B* **1998**, *102*, 1528−1538.
(46) Gandini, S. C. M.; Yushmanov, V. E.; Borissevitch, I. E.; Tabak, M. *Langmuir* **1999**, *15*, 6233−6243.
(47) Andrade, S. M.; Costa, S. M. B. *Biophys. J.* **2002**, *82*, 1607−1619.
(48) Paulo, P. M. R.; Costa, S. M. B. *Photochem. Photobiol. Sci.* **2003**, *2*, 597−604.
(49) Maus, M.; Rousseau, E.; Cotlet, M.; Schweitzer, G.; Hofkens, J.; Van der Auweraer, M.; De Schryver, F. C. *Rev. Sci. Instrum.* **2001**, *72*, 36−40.
(50) Press, W. H.; Teukolsky, S. A.; Vetterling, W. T.; Flennery, B. P. In *Numerical Recipes in FORTRAN, The Art of Scientific Computing*, 2nd ed.; Cambridge University Press: New York, 1992; p 678.
(51) O'Connor, D. V.; Phillips, D. In *Time-Correlated Single Photon Counting*; Academic Press: London, 1984; pp 43, 158.
(52) Mataga, N. *Bull. Chem. Soc.* **1957**, *30*, 375−379.
(53) Knapp, E. W.; Fischer, S. F. *Chem. Phys. Lett.* **1984**, *103*, 479−483.
(54) Knapp, E. W. *Chem. Phys.* **1984**, *85*, 73−82.
(55) Naylor, A. M.; Goddard, W. A., III; Kiefer, G. E.; Tomalia, D. A. *J. Am. Chem. Soc.* **1989**, *111*, 2339−2341.
(56) Maiti, N. C.; Ravikanth, M.; Mazumdar, S.; Periasamy, N. *J. Phys. Chem.* **1995**, *99*, 17192−17197.
(57) Akins, D. L.; Özçelik, S.; Zhu, H.-R.; Guo, C. *J. Phys. Chem.* **1996**, *100*, 14390−14396.
(58) Gouterman, M. *J. Chem. Phys.* **1959**, *30*, 1139−1161.
(59) Kasha, M.; Rawls, H. R.; Ashraf El-Bayoumi, M. *Pure Appl. Chem.* **1965**, *11*, 371−392.
(60) Kasha, M. *Radiat. Res.* **1963**, *20*, 55−71.
(61) Grad, J.; Hernandez, G.; Mukamel, S. *Phys. Rev. A* **1988**, *37*, 3835−3846.
(62) Spano, F. C.; Mukamel, S. *J. Chem. Phys.* **1989**, *91*, 683−699.
(63) Spano, F. C.; Kuklinski, J. R.; Mukamel, S. *J. Chem. Phys.* **1991**, *94*, 7534−7544.
(64) Ohno, O.; Kaizu, Y.; Kobayashi, H. *J. Chem. Phys.* **1993**, *99*, 4128−4139.
(65) Akins, D. L.; Zhu, H.-R.; Guo, C. *J. Phys. Chem.* **1996**, *100*, 5420−5425.
(66) Rubires, R.; Crusats, J.; El-Hachemi, Z.; Jaramillo, T.; López, M.; Valls, E.; Farrera, J.-A.; Ribó, J. M. *New J. Chem.* **1999**, 189−198.
(67) Micali, N.; Mallamace, F.; Romeo, A.; Purrelo, R.; Scolaro, L. M. *J. Phys. Chem. B* **2000**, *104*, 5897−5904.
(68) Yang, X.; Dai, Z.; Miura, A.; Tamai, N. *Chem. Phys. Lett.* **2001**, *334*, 257−264.
(69) Kano, H.; Kobayashi, T. *J. Chem. Phys.* **2002**, *116*, 184−195.
(70) Kano, H.; Saito, T.; Kobayashi, T. *J. Phys. Chem. A* **2002**, *106*, 3445−3453.
(71) Caminati, G.; Turro, N. J.; Tomalia, D. A. *J. Am. Chem. Soc.* **1990**, *112*, 8515−8522.
(72) Crutzen, M.; Ameloot, M.; Boens, N.; Negri, R. M.; De Schryver, F. C. *J. Phys. Chem.* **1993**, *97*, 8133−8145.
(73) Lakowicz, J. R. In *Principles of Fluorescence Spectroscopy*; Plenum Press: New York, 1983.
(74) Murov, S. L. In *Hanbook of Photochemistry*; Marcel Dekker: New York, 1973; p 55.
(75) http://www.dendritech.com/pamam.html.
(76) Welch, P.; Muthukumar, M. *Macromolecules* **1998**, *31*, 5892−5897.
(77) Lee, I.; Athey, B. D.; Wetzel, A. W.; Meixner, W.; Baker, J. R., Jr. *Macromolecules* **2002**, *35*, 4510−4520.

MA034844P